Atmos. Chem. Phys. Discuss., 10, 19277–19307, 2010
www.atmos-chem-phys-discuss.net/10/19277/2010/
doi:10.5194/acpd-10-19277-2010

Atmospheric Chemistry and Physics Discussions

Manchester Ice Nucleus Counter (MINC) measurements from the 2007 International workshop on Comparing Ice nucleation Measuring Systems (ICIS-2007)

H. M. Jones[1], **M. J. Flynn**[1], **P. J. DeMott**[2], **and O. Möhler**[3]

[1]Centre for Atmospheric Science, SEAES, University of Manchester, Manchester, UK
[2]Department of Atmospheric Science, Colorado State University, Fort Collins, Colorado, USA
[3]Institute for Meteorology and Climate Research, Karlsruhe Institute of Technology, Germany

Received: 27 July 2010 – Accepted: 2 August 2010 – Published: 16 August 2010

Correspondence to: H. M. Jones (hazel.jones@manchester.ac.uk)

Published by Copernicus Publications on behalf of the European Geosciences Union.

Abstract

An ice nucleus counter was developed and constructed to enable investigation of potential ice nucleating materials. The Manchester Ice Nucleus Chamber (MINC) is a concentric-cylinder continuous flow diffusion chamber (CFDC). A full explanation of the MINC instrument is given here, along with first results and a comparison to an established instrument of similar design (Colorado State University CFDC) during sampling of common ice nucleating aerosols at the 2007 International workshop on Comparing Ice nucleation Measuring Systems (ICIS-2007). Both instruments detected the onset of ice nucleation under similar conditions of temperature and supersaturation for several different types of ice nuclei. Comparisons of the ratio of ice nuclei to total aerosol concentrations as a function of relative humidity (RH) showed agreement within one order of magnitude. Possible reasons for differences between the two instruments relating to differences in their design are discussed, along with suggestions to future improvements to the current design.

1 Introduction

Aerosol particles may influence climate directly by the scattering and/or absorption of radiation and indirectly through their role as cloud condensation nuclei (CCN) or ice nuclei (IN). IN are defined as the subset of aerosol particles that catalyse the formation of ice crystals (Vali, 1985). The existence of atmospheric IN and the role they play in cloud formation implies that they have the ability to affect the local radiation budget; changes in cloud microphysics will change the scattering and reflective properties of cloud. Without IN, clouds would not glaciate until temperatures approach the ~-40 °C limit for homogeneous ice nucleation, with pure water droplets beginning to freeze at −36 °C (DeMott et al., 2003a; Vali, 1996). Glaciation is frequently observed at much higher temperatures due to the presence of atmospheric IN. There are currently four recognised fundamental heterogeneous ice nucleation mechanisms: deposition nucle-

ACPD
10, 19277–19307, 2010

ation, condensation-freezing, contact-freezing and immersion-freezing nucleation (Vali, 1985).

While it is recognised that ice nucleation is of critical concern for weather and climate models, there are major short-comings in our ability to treat this process reliably. One reason for this is the paucity of reliable measurements and the need for more extensive continuous measurements of IN that will ultimately allow more accurate parameterisations to be produced for use in models. There are many difficulties relating to the identification and measurement of IN. IN may act in supercooled water or supersaturated vapour, or at the interface between the two. Typical atmospheric concentrations of IN are $\sim$1 stdL^{-1} at $-20\,^{\circ}$C and $\sim$10 stdL^{-1} at $-30\,^{\circ}$C (DeMott et al., 2010a), around 6 orders of magnitude less than typical urban total atmospheric aerosol concentrations, but can be subject to very large variations in time and space. In addition, physical or chemical processes may alter the effectiveness of any given IN, (Szyrmer and Zawadzki, 1997). There are two ways in which to predict IN concentrations in models: use aerosol properties in conjunction with lab studies, or a constrained theoretical approach, on the effects of aerosol properties on ice nucleation, or, use IN climatologies of IN concentrations. When measuring IN in the laboratory or in the atmosphere, they may only be detected and counted by observing the ice crystals formed from them at given temperatures and supersaturations. The multitude of possible processes within the atmosphere makes realistic simulations of all natural atmospheric conditions within measuring systems difficult and most measurement techniques are insensitive to one or more modes of activation.

Greater interest in the research field of ice nucleation is being spurred by the increasing demand for knowledge concerning ice clouds in the atmosphere and the important contribution they make to regional and global hydrological pathways. Although secondary ice formation mechanisms like the Hallett-Mossop process (Hallett and Mossop, 1974) can be extremely important for the ultimate glaciation of clouds warmer than $-8\,^{\circ}$C, ice nuclei are likely the cause of initial glaciation (with the exception of glaciation by homogeneous freezing or the 'seeder-feeder' mechanism, see

ACPD
10, 19277–19307, 2010

Bergeron, 1965). Measurements of IN are therefore of paramount importance in order to obtain information concerning their abundance, activity, constituents and major regional global sources as well as their temporal diurnal and seasonal variations; without these measurements, accurately predicting ice cloud initiation and development in particular meteorological situations will remain a limiting factor to providing better weather and regional climate prediction models.

This paper describes a Continuous Flow Diffusion Chamber (CFDC) instrument developed for field and laboratory use at the University of Manchester. Details of the operation principles, hardware and software are given. Calibration and operational procedures are also outlined. Initial results obtained at the International Workshop on Comparing Ice Nucleation Measuring Systems – 2007 (ICIS-2007) (see Section 3), along with a comparison to other instruments present at the workshop are shown and discussed. Suggestions for future development are outlined in Sect. 6.

2 The Manchester Ice Nucleus Chamber (MINC)

Previous work on IN measurements at the University of Manchester included the design and construction of flat-plate continuous flow diffusion chambers, initially of horizontal configuration and later of vertical configuration (Hussain and Saunders, 1984) in an attempt to reduce particle losses in the chamber. Results from these chambers were used as part of the IN parameterisation developed by Meyers et al., (1992), a parameterisation, or derivations thereof, still widely in use. However, these early flat plate instruments were found to suffer edge effects and were bulky, making them difficult to transport and unsuitable for aircraft use, although recent flat-plate designs appear to have resolved these problems (e.g. Stetzer et al., 2008). As a consequence of this previous work, the Manchester Ice Nucleation Chamber (MINC) was designed as a Continuous Flow Diffusion Chamber (CFDC) of the cylindrical design based on the laboratory instrument first described in Rogers (1988) and the main aspects of this design are described below.

ACPD
10, 19277–19307, 2010

2.1 Principle of operation

In MINC, supersaturated conditions are established between the ice-coated walls of two vertically-orientated, concentric cylinders maintained at different temperatures. In the region between the two ice-covered walls, almost linear steady-state vapour pressure and temperature fields are established. Equilibrium vapour pressure is an exponential function of temperature and therefore the region between the walls is supersaturated with respect to ice, with the degree of supersaturation determined by the temperature difference between the walls and the distance from the walls (Rogers, 1988). Humidities from ice saturation to well in excess of water saturation can be achieved with this system. Sample air is injected into the central region of laminar flow at the top of the chamber, sandwiched between two layers of dry, filtered air. This ensures that the sample environment is narrow and well defined. It is important that the flow be laminar so that the sample environment can be accurately determined. Poiseuille flow within the chamber results in a parabolic velocity profile due to the wall separation being small compared to the cylinder radii (Knudsen and Katz, 1958). In the older horizontal flat plate designs, the aerosol laminar remained centred between the plates, but with vertical chambers there is the added complication of buoyant circulation due to the temperature gradient, (Sinnarwalla and Alofs, 1973): air near the cold wall will tend to sink; air near the warm wall will tend to rise. This results in a skewed velocity profile and displacement of the lamina and maximum supersaturation region towards the cold wall. If the temperature difference between the walls becomes too great then negative flow may result. This could lead to undesirable influences on the sample air stream so the flow conditions are monitored in real-time using calculations given by Rogers (1988). An "evaporation section" at the bottom of the chamber uses an non-cooled plastic outer (warm) wall while retaining the cold and ice-covered cold wall to allow the vapour and temperature fields to relax to the cold wall conditions, with the intent to keep the air slightly supersaturated with respect to ice but not with respect to water. This allows any water droplets formed in the first part of the chamber to be removed

ACPD
10, 19277–19307, 2010

by either the Bergeron-Findeisen process (e.g. Rogers and Yau, 1989) whereby ice crystals grow at the expense of water droplets (fairly minor), or by diffusional loss of vapour to the cold wall. Detection of ice crystals by particle size only using an optical particle counter (OPC) is then possible.

2.2 Instrument design

The MINC instrument is housed inside a rail frame (Bosch), 159 cm×72 cm×20 cm. The instrument, pre-mounted in the frame, can be transported and located in the laboratory or in the field. The following sections outline the construction and design elements of various MINC components.

2.2.1 The chamber

The chamber itself consists of two vertical, concentric copper cylinders (1 mm wall thickness) with outer diameters of 98 mm and 76 mm, between which exists a 10 mm annular gap. It is in this gap that supersaturated conditions are developed as described in Sect. 2.1. This annular arrangement avoids the edge effects present in chambers of the flat-plate design, and the vertical arrangement avoids gravitational loss of particles. To increase the hygroscopicity of the wall surface, to allow a smooth ice layer to be applied, the walls were treated with an 'ebonizing' solution that reacts with the copper to form a thin layer of black cupric sulphide crystals (see Rogers et al., 2001). The total length of the chamber is 750 mm, with the bottom 250 mm of the outer wall made of insulating hydrophobic plastic; this is the water droplet evaporation zone. Residence time in the system (from instrument inlet to detection system) is ∼10 s, during which time crystals may grow in the chamber and then be detected by passing through a particle counter at the exit of the chamber. The wall temperatures are monitored using thin film Platinum Resistance Thermometers (PRTs, class A, 4-wire PT-100, ±0.15 °C) at three positions along each wall; they are henceforth labelled top, middle and bottom, for the inner and outer wall. The chamber is insulated with aluminium coated bubble

ACPD
10, 19277–19307, 2010

wrap (modern roof-space insulation) and then Armaflex insulation sheeting that also prevents condensation. This is all encapsulated inside a metal frame box and fixed to the rack to increase stability.

With instruments of this design, there are two main design issues that must be accounted for: wall effects and transient supersaturations. Wall effects (loss of aerosol to chamber walls) can be minimised by keeping the aerosol laminar away from the walls and using a large aspect ratio (width:height), (e.g. Elliott, 1971). Transient supersaturations need to be avoided as they momentarily increase the local supersaturation potentially activating some aerosol particles which would have otherwise remained inactivated, thus giving false readings. This problem can be minimised in two ways, either by preconditioning the sample (e.g. Saxena et al., 1970) or delaying the vapour diffusion region until conditions are settled (Fukuta and Saxena, 1979). The current design uses both preventative methods by recycling the cold dry sheath air, drying the incoming sample air and leaving the top 10 cm of chamber ice free.

2.2.2 The refrigeration system

The temperature of each wall is controlled independently by its own refrigeration system, see Fig, 1. Each system is required to provide a stable steady temperature along the length of the chamber wall. Copper tube (3/8 in outer diameter, 1 mm wall thickness) is soldered to the outside of the copper section of the outer wall in a coil arrangement, with a 5 cm space between each coil. The inner coil stretches the full length of the inside wall, it is not soldered to the wall due to spatial constraints, but is immersed in heat transfer fluid (Polydimethyl Siloxane) to increase the thermal contact with the wall. All externally exposed refrigeration pipes are insulated with Armaflex tubing to avoid reducing the efficiency of the refrigeration system and to minimise frosting. Two compressor units (Electrolux, CML90FB3) – one for each wall circulate R404A refrigerant around each system. An electronic expansion valve (Sporlan, SEI 0.5-10-S) connected to the outlet of each compressor is controlled by the user and determines the temperature of the coil, and hence the chamber wall. Refrigerant pressure is mea-

ACPD
10, 19277–19307, 2010

sured (Sensortechnics, CTE9020GY4) before and after the coil, and a second expansion valve after the coil is used to maintain the pressure across the coil. Equalised pressure results in equal cooling along the wall, and so a steady wall temperature.

2.2.3 The airflow system

Sample air (1 LPM) initially passes through the inlet system, which consists of an impactor (design as per Rogers et al., 2001) that has a nominal 1.3 µm 50% cut-off to remove larger particles and a counter-flow gas drying column (Permapure Nafion, PD-100T) to remove any moisture from the sample that would result in frosting of the inlets and consequently lead to false readings due to ice splinter formation and release into the sample stream. There is also a system of valves that allow a zero particle filter to remove incoming particles to the impactor and so allow a background test to ensure there is no frosting in the chamber. A pressure relief valve is also positioned at the top of the chamber for use during the wall icing process. As outlined in Sect. 2.1, this sample air enters the chamber between two layers of dried, particle free air (4.5 LPM each). The sheath air is dried by passing it through a desiccant drying column (Drierite, size 8 mesh) and then filtered using a clean-room grade filter (HEPA, removing at least 99.97% of airborne particles 0.3 µm in diameter), see Fig. 1. Air passed through the air flow pump provides the counter-flow to the inlet drier, and then passes through a second drier and filter before being split into the two sheath flows and an exhaust flow. The airflow system is closed, such that air flowing out of the bottom of the chamber (10 LPM) is recirculated and the exhaust flow is equal to the inlet flow.

2.2.4 The detection system

Ice crystals are expected to grow up to sizes of ~10 µm (Rogers, 1988), depending on sample temperature and supersaturation, during an approximate chamber residence time of 10 seconds (with 6 s exposure to steady state experiment conditions). The growth of ice crystals to sizes larger than the incoming aerosol sizes, and the evapo-

ACPD
10, 19277–19307, 2010

ration of any water droplets that form in cases when operating above water saturation, allows the reliable detection of ice crystals based on particle size. Air exiting from the bottom of the chamber is immediately drawn through an optical particle counter (OPC, CLiMET 3100-1158) modified by the removal of an internal critical orifice to operate at 10 LPM, to detect and size crystals.

2.2.5 Software

A LabVIEW program is used to monitor and record data from the CFDC. Wall temperatures, refrigeration pressures, air flow temperatures, air pressure, air flow rates and OPC data are constantly monitored to ensure correct operation and the data are recorded. The program also allows the user to control the refrigeration valves.

2.3 Calibration

2.3.1 Aerosol losses

Due to the nature of the sample inlet system, described in Sect. 2.2.3, size dependent losses are expected. A Topaz aerosol generator was used to produce a distribution of ammonium sulphate particles that was then measured by a Differential Mobility Particle Sizer (DMPS, Williams et al., 2007) before and after the inlet system. Total aerosol concentrations during these tests were of the order of 10^6 particles per cubic centimetre. During these tests, the counterflow to the drier was provided by the MINC airflow system, while the sample flow was provided by a Condensation Particle Counter (CPC, TSI 3025A) in the DMPS system. Based on this information, see Fig. 2, a correction was applied to the measured data to account for losses in the inlet system. Transmission efficiency was assumed to be 40% between 500 nm and 1 µm, then the impactor transmission curve is applied (see below for description). This low transmission efficiency curve is primarily due to diffusional losses of smaller particles in the Nafion dryer, and impaction losses of larger particles in the impactor and also in the connec-

ACPD
10, 19277–19307, 2010

tions between inlet parts. Coagulation is not thought to play a role here.

The impactor 50% cut-off was tested by the use of a Grimm model 1.108 aerosol particle counter sampling laboratory air before and after the impactor. The 50% cut-off was found to be at 1.3 µm, with 75% transmission at 0.8 µm and 25% transmission at 1.7 µm.

2.3.2 Wall temperature

As the temperature of each wall was not measured directly at the ice surface, it was important to know how the recorded temperatures (measured at the back of the copper surface) related to the ice surface temperature. Calibrated PRTs were placed against the dry copper wall inside the chamber at corresponding positions to the measurement PRTs on the outside copper surface. The walls were then cooled/warmed under conditions typical of those used at ICIS-2007. Airflow was present to ensure representative results. This test was performed at three different start temperatures to investigate whether there was a dependence on starting temperature. Results of this calibration showed that a common straight-line-fit could be used for each set of PRTs, indicating that starting temperature did not influence the results. Outer wall measurement temperatures agreed with calibration PRT temperatures to within 0.5 °C. The inner wall calibration temperatures were found to be much higher than the measurement PRTs indicated, especially when operating the instrument at very low temperatures (e.g. −40 °C). The top of the chamber showed the most discrepancy, with a difference of 2 °C at −20 °C and 5 °C at −40 °C. The mid point of the inner chamber wall showed the lowest discrepancy with 0 °C difference at −20 °C and 3 °C at −40 °C. As such, this calibration was very important for the accurate determination of the sample temperature and hence supersaturation. This calibration was included in the chamber operation software. Investigations using extra PRTs along the length of each wall showed that wall temperatures were steady along the walls, but with measurable departures within ∼10 cm at each end, reducing the aerosol exposure time to steady state experimental conditions from ∼6 s to ∼4 s.

ACPD
10, 19277–19307, 2010

2.3.3 Optical particle counter

The Optical Particle Counter (OPC) used was a CLiMET 3100-1158. As the OPC was operated at a higher flow rate than standard, a peak voltage to size calibration was carried out by Optical Science Ltd. using polystyrene latex (PSL) spheres and a standard oscilloscope. The OPC outputs two continuous analogue signals – high gain and low gain, from which concentrations of 1–2 µm particles and 3–8 µm particles respectively were derived. The counting efficiency of the high gain channel is reported as 50% ±10% at 0.5 µm, whereas the low gain channel counting efficiency is reported as 100% ±10% for 0.8 µm particles The OPC sampled the total flow from the chamber. Ice numbers detected in the total flow are related to the sample flow to determine nucleated IN number concentrations. Comparator electronics and Schmidt triggers were used to detect and bin analogue pulses representing individual particle output from the CLiMET. The PSL calibration curve was used to set threshold levels on the comparator electronics. Particle events in each size bin were counted using an 8 channel pulse counter card (National Instruments, 6602) in the control computer. To confirm the calibration was satisfactory and the pulse counter system was operating correctly, the modified CLiMET complete with comparator electronics and pulse counter was compared in the laboratory to a calibrated OPC (Grimm Aerosol Tecnik, Dust Monitor 1.105, optical scattering size range 0.5–20.0 µm) and an Aerodynamic Particle Sizer (TSI APS 3321, aerodynamic size range 0.5–20.0 µm). A Vibrating Orifice Aerosol Generator (VOAG) was used to produce monodisperse aerosol at known sizes (3, 4, 5 µm) for use in this comparison. Solutions using NaCl, oleic acid and olive oil were used. Results showed that measured size distributions from all instruments peaked at the same size to within 1 µm, but that the CLiMET exhibited a broader distribution than the other instruments, typically spanning over three size channels, equivalent to the peak size +/- 2 µm. The APS has higher resolution due to many more channels than the CLiMET, and the distribution tended to span over ~6 size channels, roughly equivalent to peak size −1/+2 µm. GRIMM OPC results were harder to discern due to

ACPD
10, 19277–19307, 2010

the smaller number of size bins and the staggering of the bin sizes. Typically, peaks spanned two or three size bins, e.g. when measuring 5 µm, sizes from 3.5 – 7.5 µm were seen.

3 International workshop on Comparing Ice nucleation measuring Systems (ICIS) 2007

The International workshop on Comparing Ice nucleation measuring Systems (ICIS) 2007, also dubbed the Fourth International Ice Nucleation Workshop, was held at the Aerosol, Interactions and Dynamics in the Atmosphere (AIDA) chamber facility at the Institute for Meteorology and Climate Research (IMK), Karlsruhe Institute of Technology (KIT), Germany. The main objective of this workshop was to compare and contrast currently existing ice nucleation measurement instruments using a common, well characterised, aerosol generation system, a revived concept from earlier workshops, the third being in Laramie, Wyoming, 1975, (Vali, 1975). The purpose of this was to assess the range and consistency of present IN measurement capabilities. Details of all instruments and their respective research groups are given in the ICIS-2007 overview paper (Möhler et al., 2008; DeMott et al., 2010b). Experiments were carried out between 17 September 2007 and 28 September 2007. Aerosol samples were chosen for their expected ice nucleation properties, details of which are summarised in Table 1.

Samples were prepared so that the vast majority of particles used in the experiment were <1 µm diameter; thus allowing those instruments without impactors on their inlets to identify IN more easily based only on measured particle size. Aerosol particles were introduced to the Aerosol Preparation and Characterisation (APC) Chamber at typical initial concentration of up to $10^5\,cm^{-3}$. IN detection instruments could then sample directly from this chamber, during sampling number concentrations were typically at or below around $10^4\,cm^{-3}$. After aerosol size characterisation, a minor fraction of the aerosol was transferred to the much larger AIDA chamber (resulting in concentrations of $\sim 500\,cm^{-3}$) for cloud nucleation expansion experiments. There was an

ACPD
10, 19277–19307, 2010

opportunity for sampling from the AIDA chamber prior to an expansion run. The AIDA chamber walls were pre-coated with ice to establish ice saturation at wall temperature. The whole chamber was cooled to sub-zero temperatures, and then the air inside the chamber was further cooled by adiabatic expansion, e.g. Möhler et al., 2003. During an expansion, a suite of instruments including particle counters are used to determine the activation point and evolution of ice nucleation as a function of temperature and supersaturation. AIDA expansion experiments were carried out for all samples in Table 1. Further information can be found in Möhler et al., 2008.

4 Results

During ICIS-2007, the MINC instrument sampled directly from the APC. The MINC was operated to measure ice nuclei concentrations while slowly increasing relative humidity (RH), or equivalently supersaturation, at steady sample temperatures between −15 and −33 °C. These "supersaturation scans" were performed by lowering the inner wall temperature and increasing the outer wall temperature from a common start temperature; this process is entirely manual and required close monitoring. As can be seen in Fig. 3, the sample temperature can vary by ∼1 °C over a supersaturation scan. Each scan took up to 30 min to complete. Faster scans are possible but this would be at the expense of accuracy in determining the fraction of particles activating at specific T and RH conditions. Testing during ICIS-2007 showed that MINC can operate at supersaturations up to 6% (with respect to water) at −25 °C before water droplets are able to pass through the droplet evaporation zone at sizes large enough to be counted. At ICIS-2007, the aim was to scan up to 5% supersaturation with respect to water. Unfortunately, as temperature calibrations were carried out post-workshop, supersaturation scans very rarely passed water saturation.

Results were obtained by MINC for all samples listed in Table 1 except the live bacteria sample. While MINC did sample the soot aerosol samples, the temperatures required for these soot samples to be effective IN were much lower than those which

ACPD
10, 19277–19307, 2010

could be achieved in MINC and so are not reported here.

5 Detection of IN

MINC was successfully operated and tested for the first time at ICIS-2007 on 17 September 2007. Figure 3 shows a time series of sample temperature, supersaturation and the number of particles >3 µm detected by the CLiMET counter when measuring Arizona Test Dust (ATD). This is the real-time information available to the user when operating the MINC. To allow comparison with other instruments, MINC results are typically plotted as activated fraction against supersaturation with respect to water, where the activated fraction is defined here the as number of particles >3 µm divided by the total number of particles initially entering the instrument. Total aerosol concentration was measured by a CPC as part of the APC system, size distribution was measured by an SMPS and APS and corrected using the following method: The measured transmission curve (Fig. 2) was applied to the measured size distributions. Subsequent integration of corrected and uncorrected size distributions gave a transmission coefficient of around 0.55 for ATD samples (0.57 for SD and 0.63 for Snomax®). These transmission coefficients were then applied to the total aerosol number used in calculating IN activated fractions. The 3 µm threshold was used due to the limitations imposed by the optical particle counter.

5.1 Results at different temperatures

ATD was tested on three days and several RH-scans were performed over this period. Sample temperatures were −31, −28, −26 and −25 °C, results are shown in Fig. 4. The key result here was that at lower sample temperatures, lower supersaturations were required for the activated fraction to rise above the background. An inverse temperature dependence to active fraction was also noted. Similar results were seen for the other samples.

ACPD
10, 19277–19307, 2010

5.2 Comparison of MINC measurements with those from other instruments

The main aim of the workshop was to compare IN measurements by all the instruments present at the workshop, here the MINC results are compared to the CSU-CFDC instrument. This is a natural comparison since MINC is similar in many key aspects (e.g. geometry, inlet) to the CSU-CFDC design of Rogers et al. (2001) and unpublished modifications since that time. Like MINC, the CSU-CFDC includes separate compressors and digital expansion valves for cooling the two walls. It differs from the 2001 design and from MINC primarily in possessing an actively cooled and iced outer wall in the evaporation section, and no heat transfer fluid within the inner wall, where copper coils now directly attach to the inside wall surface. The two chambers also differ in length, with MINC having a total length of 75 cm and CSU-CFDC having a total length of 81 cm, with a reduced length of non-iced section below to inlet manifold. In addition, although the design elements to the sample inlet section are the same, the physical arrangement and actual components are different such that MINC experiences lower transmission efficiencies than CSU-CFDC (0.8–0.9 for particles >100 nm). The main difference in the inlet system is the use of a Nafion dryer in the MINC system, where the losses experienced are much more extreme compared to the diffusion driers used in the CSU-CFDC system. This instrument is the same version (CFDC-1H) used in recent laboratory and field studies, e.g., Eidhammer et al., 2010; Richardson et al., 2010. Both instruments were operated as described in Sect. 4. Throughout each day, several RH-scans were performed at different temperatures. Where possible, MINC performed scans at temperatures matching those of the CSU-CFDC to allow easier comparison between these instruments.

Results for ATD comparisons are shown in Fig. 5 for two sample temperatures (~−25 °C and ~−32 °C); Fig. 5 also shows the CSU-CFDC activated fractions recalculated using an activated ice size threshold of 3 µm to simulate the MINC detection threshold. CSU activated fractions determined using the 3 µm threshold are much closer to the MINC data, particularly at higher values of RH_{water}, e.g. at 102% RH_{water}

ACPD
10, 19277–19307, 2010

activated fraction is reduced by 50%. However, this change was found to make only a modest difference (up to 1%) in the RH values attributed to activation, and is well within measurement uncertainties. Figure 5a shows activated fraction from CSU-CFDC scans under similar conditions varying by up to a factor of 5, MINC data varies from CSU-CFDC data by a similar amount, though points follow similar activated fraction versus RH_{water} curves. Figure 5b shows results from −32 °C, where much closer agreement between the results can be seen, especially above 95% RH_{water} and active fractions exceeding 10^{-3}. Figure 6 plots the supersaturation (as RH_{water}) at which an activated fraction of 1 in 1000 was recorded as reported by both MINC and CSU-CFDC for three different samples during ICIS-2007 as a function of sample temperature. This plot highlights the good agreement between the two instruments in determining the supersaturation at which IN activation begins at any given temperature.

6 Discussion

The MINC instrument performed successfully during first measurements at the ICIS-2007 workshop. Post workshop wall temperature calibration revealed that most scans did not reach much higher than 100% RH_{water}: this restricts the number of RH scans where activated fraction can be compared with that reported by some of the other groups at the workshop. Figure 4, showing results solely from MINC for ATD samples, clearly highlights the dependence of IN activity on temperature and supersaturation.

Variations in activated fraction measured by the same instrument under apparently similar conditions as highlighted in Fig. 5a may reflect spatio-temporal differences in the properties of the sample aerosol in the APC. For example the C-5-3785 curve in Fig. 5a is data from the morning of 17 September 2007, while the C-6-5875 curve is from the afternoon. Between these measurements being made the APC had been flushed and refilled with a fresh ATD sample. Even when the APC was not refilled between scans the aerosol population within it evolved with time. MINC data shown in Fig. 5a were taken in the afternoon. If it is assumed that larger particles are more efficient IN than

ACPD
10, 19277–19307, 2010

smaller particles, then the differences in the transmission efficiencies between the two instruments are important, particularly if the resultant aerosol size distribution sampled by the MINC has comparatively less larger particles, thus affecting the measured AF.

Figure 7 shows the typical variation in aerosol properties in the APC throughout the day. Figure 7a shows how the total aerosol concentration varied with time and figure 7b shows size distributions (normalised to maximum value) at various times during the day, see caption and also dashed lines on figure 7a. As can be seen, the peak of the size distribution is shifting to slightly higher sizes throughout the day as the total concentration decreases significantly. These physical changes in the aerosol population are probably the result of particle coagulation and losses.

The MINC scans shown on figure 5a while taken on the same day as the CSU scans were not performed at the same times, being separated by 1 h 20 min. Additionally MINC and CSU-CFDC sampled from different levels of the APC during ICIS-2007 so results may also be affected by any stratification that occurred in the chamber as each instrument could have effectively been measuring different aerosol, although a mixing ventilator should have achieved homogeneous aerosol distribution throughout the chamber. These data show that measured activated fraction is very sensitive to the properties of the sample aerosol distribution (even for what should be the same sample) as well as the T and RH conditions under which the IN measurement is made. Such variations in sample properties must be taken into account when comparing different instruments and efforts should be made minimise these effects when conducting inter-comparison experiments.

When similar scans were performed at similar times as was the case for the −32 °C comparison shown in Fig. 5b there was very good agreement between the results. On these scans the CSU-CFDC appeared to detect deposition nucleation at lower RH which was not detected by MINC, this could be due to the differences in the design of the evaporation region or the longer transit time (and exposure to the vapour field) in the CSU instrument. This result could as well reflect onset conditions, at a temperature just moderately colder, for deposition nucleation, which was noted to become more

ACPD
10, 19277–19307, 2010

dominant for ATD aerosols as temperature decreased toward −40 °C in the CSU results (Koehler et al., 2010).

Comparisons of T and RH conditions for IN activation to begin (defined here as an activated fraction of 1 in 1000), determined with both MINC and CSU-CFDC for experiments performed using three different samples showed very good agreement between the instruments (see Fig. 6). Data points for each of the sampled followed a separate trend, R^2 values from trend lines plotted through collective MINC and CSU-CFDC data points are 0.93, 0.78 and 0.95 for ATD, SD and SM data respectively. Figure 6 also shows the CSU-CFDC results using the 3 µm activation threshold for the ATD sample, and it can be seen that these data points are in most cases almost indistinguishable from the standard CSU-CFDC data.

During the AIDA workshop elevated laboratory temperatures compared with those at the University of Manchester led to increased difficulties in obtaining constant wall temperatures along the length of the chamber. As discussed in section 2.3.2 tests with additional temperature sensors carried out post workshop revealed end effects extending over about 10 cm at each end of the chamber with a constant temperature region between. These experiments indicated that the middle temperature sensors should be used to determine sample temperature and supersaturation, and that the sample was exposed to the desired conditions for ∼4 s rather than ∼6 s as would have been the case under ideal conditions.

In addition to variability in the sample aerosol in some experiments, discrepancies in the results between the MINC and CSU-CFDC instruments could be due to some, or all, of the following potential issues. The modified CLiMET counter is expected to encounter significant dead time issues with particles concentrations of several tens of thousands per litre: this is not an issue when measuring under atmospheric conditions, but a definite issue when sampling during ICIS-2007. Differences in the way the signal from the CliMET was handled by the two instruments may lead to some differences in reported counts under these conditions. Secondly, the choice of threshold for determining the presence of IN within the chamber should be linked to the impactor

ACPD
10, 19277–19307, 2010

cut-off (1.3 µm for MINC) however, due to difference in dead-time between the two gain stages on the CliMET, data could only be used from the low gain channel, limiting the MINC threshold to 3 µm. The CSU instrument typically uses a 2 µm threshold. When the CSU data were re-analysed using a 3 µm threshold this did bring the results into closer agreement (less than a factor of 5 difference as seen in Fig. 5), although it is important to consider other sampling issues that may have existed. Two of the major differences between the two instruments compared here is the length of the chamber and the water droplet evaporation section. The CSU-CFDC has a longer chamber and therefore additional ice crystal growth time, and has an actively-cooled evaporation section. The MINC has a passive evaporation section, which in the high temperatures experienced at ICIS-2007 could have resulted in the evaporation of ice crystals, and thus fewer crystals reaching the detection threshold. Despite these differences, when considering sample temperatures and supersaturation at the point where the activated fraction reaches 1 in 1000, the results from the MINC and CSU instruments show excellent agreement, with instrument-instrument variability similar in magnitude to sample–sample variability.

6.1 Improvements to current design

While operating the MINC during the workshop, and when comparing the data produced with other instruments it became apparent that the current instrument had a number of limitations which could be overcome in future builds by modification of the design. Suggestions for improvements to the current design which should help to overcome the difficulties reported at ICIS-2007 are listed here: The chamber should be made longer to extend IN exposure time – it is suggested that the chamber be lengthened to 81 cm total length to allow easier comparison to existing instruments; Steps should be taken to improve the uniformity of wall temperatures – these might include increasing the number of refrigeration coils on both walls and improving the thermal contact between walls and coils; Extra temperature sensors down the length of both walls would increase the knowledge of and help constrain the sample conditions and

ACPD
10, 19277–19307, 2010

subsequent calculations; Sample and sheath flows should be pre-cooled prior to entering the chamber thus reducing transient conditions at the top of the chamber, this can be achieved using a sub-coil from the refrigeration system. The refrigeration systems should also be modified to allow experiments at lower temperatures. The current passive water droplet evaporation region, should be replaced with an active evaporation section where the outer wall in this section is cooled to the same temperature as the inner wall – this would allow accurate determination of the conditions in the last section of the chamber; an improved higher resolution particle detection system is required, ideally one capable of phase discrimination in addition to producing size distribution information.

7 Conclusions

Initial results from the Manchester Ice Nucleation Counter (MINC), collected during the ICIS-2007 workshop are reported here. Measurements of ice nuclei are compared to the results from the CSU-CFDC instrument, which is of similar design. Results show that MINC and CSU-CFDC detected similar numbers of IN in the samples shown while performing comparable RH-scans. For RH-scans performed at similar temperatures, activated fraction at any given RH value agreed to within one order of magnitude (worst case), and usually showed much closer agreement in activated fractions of different IN within RH measurement uncertainties. Several suggested improvements to the current MINC set-up, based on knowledge gained at the workshop, are described in Sect. 5.1 of this paper. It is particularly evident, when using a threshold size for ice detection, that increasing growth time and reducing evaporative losses will increase the activated fraction that a CFDC detects, especially in the water supersaturated regime. The move to better ice crystal detection by phase detection of smaller particles, if feasible, would seem advantageous for IN detection systems because the need to grow ice crystals to much larger sizes than the largest sampled aerosol particle is not required. Successful phase detection of much smaller particles could remove the need for aerosol selection

ACPD
10, 19277–19307, 2010

at the inlet (although problems may arise between misclassification of aerosol particles as ice crystals) and the need for a water droplet evaporation section as water droplets and ice crystals could be classified. These results show that the workshop has been successful in both providing excellent knowledge exchange between groups in this difficult area of research and that IN measurements in future will have a common basis for comparison following recommended improvements in current measurement systems.

Acknowledgements. Thanks to Paul Williams and workshop staff at The University of Manchester. First author would like to thank Tony Prenni from CSU for his support, particularly during the development stages. The Karlsruhe Institute of Technology provided funding during ICIS-2007 for the facility infrastructure within the Helmholtz Research Programme "Atmosphere and Climate". We acknowledge Ottmar Möhler and Olaf Stetzer for their roles in co-organizing the ICIS-2007 workshop. Thanks to the AIDA staff members for their support during the ICIS-2007 workshop. We also thank Thomas Schwartz (Karlsruhe Institute of Technology) for support in preparing the bacterial cultures, Eli Ganor (Tel Aviv University) for providing the Israeli dust sample, and Hans Moosmüller (Desert Research Institute) for providing the Canary Island dust sample. Collaborative work with the UK Met Office was funded by the DIAC-UKAAN Aerosol Knowledge Transfer program. Attendance to the ICIS-2007 workshop was funded by the ACCENT Access to Infrastructures Program, the University of Manchester contribution to the workshop was funded by NERC. Attendance at the 2008 results workshop was funded by ESF/INTROP. Paul DeMott acknowledges funding support for this research from the US National Science foundation grant ATM-0611936.

References

Bergeron, T.: On the low-level redistribution of atmospheric water caused by orography, in: Suppl. Proceedings of the International Conference on Cloud Physics, Tokyo and Sapporo, 24 May–1 June, 96–100, 1965.

DeMott, P. J., Petters, M. D., Prenni, A. J., Carrico, C. M., Kreidenweis, S. M., Collett, J. L., and Moosmüller, H.: Ice nucleation behavior of biomass combustion particles at cirrus temperatures, J. Geophys. Res., 114, D16205, doi:10.1029/2009JD012036, 2009.

ACPD

10, 19277–19307, 2010

DeMott, P.J., Prenni, A. J., Liu, X., Kreidenweis, S. M., Petters, M. D., Twohy, C. H., Richardson, M. S., Eidhammer, T., and Rogers, D. C.: Predicting global atmospheric ice nuclei distributions and their impacts on climate, Proc. Natl. Acad. Sci., 107(25), 11217–11222, 2010a.

DeMott, P. J., Möhler, O., Stetzer, O., Murakami, M., Leisner, T., Bundke, U., Klein, H., Kanji, Z., Cotton, R., Jones, H., Petters, M. D., Benz, S., Brinkmann, M., Rzesanke, D., Saathoff, H., Nicolet, M., Gallavardin, S., Saito, A., Nillius, B., Bingemer, H., Abbatt, J., Ardon, K., Levin, Z., Ganor, E., Georgakopoulos, D. G., Saunders, C., and Vali, G.: Resurgence in ice nuclei measurement research, B. Am. Meteorol. Soc., in review, 2010b.

Eidhammer, T., DeMott, P. J., Rogers, D. C., Prenni, A. J., Petters, M. D., Twohy, C. H., Rogers, D. C., Stith, J., Heymsfield, A., Wang, Z., Haimov, S., French, J., Pratt, K., Prather, K., Murphy, S., Seinfeld, J., Subramanian, R., and Kreidenweis, S. M.: Ice initiation by aerosol particles: Measured and predicted ice nuclei concentrations versus measured ice crystal concentrations in an orographic wave cloud, J. Atmos. Sci., in press, doi: 10.1175/2010JAS3266.1, 2010.

Elliott, W. P.: Dimensions of thermal diffusion chambers. J. Aerosol Sci., 28, 810–811, 1971.

Fukuta, N. and Saxena, V. K.: Horizontal Thermal-Gradient Cloud Condensation Nucleus Spectrometer, J. Appl. Meteorol., 18(10): 1352 – 1362, 1979.

Knudsen, J. G. and Katz, D. L.: Fluid dynamics and heat transfer, McGraw Hill, New York, USA, 576 pp., 1958.

Meyers, M. P., DeMott, P. J., and Cotton, W. R.: New primary ice-nucleation parametrisations in an explicit cloud model, J. Appl. Meteorol., 31(7), 708–721, 1992.

Koehler, K. A., Kreidenweis, S. M., DeMott, P. J., Petters, M. D., Prenni, A. J., and Möhler, O.: Investigations of the impact of natural dust aerosol on cold cloud formation, Atmos. Chem. Phys., in preparation, 2010.

Möhler, O., Stetzer, O., Schaefer, S. Linke, C., Schnaiter, M., Tiede, R., Saathoff, H., Kramer, M., Mangold, A., Budz, P., Zink, P., Schreiner, J., Mauerberger, K., Haag, W., Karcher, B., and Schurath, U.: Experimental investigation of homogeneous freezing of sulphuric acid particles in the aerosol chamber AIDA, Atmos. Chem. Phys., 3, 211–223, doi:10.5194/acp-3-211-2003, 2003.

Möhler, O., DeMott, P. J., Stetzer, O., and the ICIS-2007 team.: The Fourth International Ice Nucleation Workshop ICIS-2007, Proceedings to the 15th International Conference on Clouds and Precipitation, Cancun, Mexico, 7–11 July, 2008.

Richardson, M. S., DeMott, P. J., Kreidenweis, S. M., Petters, M. D., and Carrico, C. M.: Obser-

ACPD
10, 19277–19307, 2010

vations of ice nucleation by ambient aerosol in the homogeneous freezing regime, Geophys. Res. Lett., 37, L04806, doi:10.1029/2009GL041912, 2010.
Rogers, D. C.: Development of a continuous flow thermal gradient diffusion chamber for ice nucleation studies, Atmos. Res., 22, 149–181, 1988.
Rogers, D. C., DeMott, P. J., Kreidenweis, S. M., and Chen, Y. L.: A continuous-flow diffusion chamber for airborne measurements of ice nuclei, J. Atmos. Ocean. Tech., 18(5), 725–741, 2001.
Saxena, V. K., Burford, J. N., and Kassner, J. L.: Operation of a Thermal Diffusion Chamber for Measurements on Cloud Condensation Nuclei, J. Atmos. Sci., 27(1), 73–75, 1970.
Sinnarwalla, A. M. and Alofs, D. J.: A cloud nucleus counter with long available growth time, J. Appl. Meteorol., 12, 831–835, 1973.
Stetzer, O., Baschek, B., Luond, F., and Lohmann, U.: The Zurich Ice Nucleation Chamber (ZINC) – A new instrument to investigate atmospheric ice formation, Aerosol Sci. Tech., 42, 64–74, 2008.
Szyrmer, W. and Zawadzki, I.: Biogenic and anthropogenic sources of ice forming nuclei: A review, B. Am. Meteor. Soc., 78(2), 209–228, 1997.
Vali, G.: Nucleation Terminology, B. Am. Meteor. Soc., 66, 1426–1427, 1985.
Vali, G.: Ice Nucleation Workshop, Summary Report, University of Wyoming, Laramie, USA, 18 pp., 1975.
Williams, P. I., McFiggans, G., and Gallagher, M. W.: Latitudinal aerosol size distribution variation in the Eastern Atlantic Ocean measured aboard the FS-Polartern, Atmos. Chem. Phys., 7, 1–11, doi:10.5194/acp-7-2563-2007, 2007.

ACPD
10, 19277–19307, 2010

Table 1. ICIS-2007 sample information.

Date	Sample	Notes
17/09/07	ATD	Commonly used in past IN studies. Mechanically produced by PTI. Representative of SW US desert dust
18/09/07		
19/09/07		
20/09/07	Soot	Generated by graphite spark generator
21/09/07		
24/09/07	Israeli Dust	Collected sample after Israeli dust storm
25/09/07	Saharan Dust	Collected sample from near Cairo
26/09/07	Canary Island Dust	Collected sample from region exposed to deposition from Saharan aerosol layers
27/09/07	Snomax®	Manufactured IN protein
28/09/07	Live Bacteria	Pseudomonas syringae

ACPD
10, 19277–19307, 2010

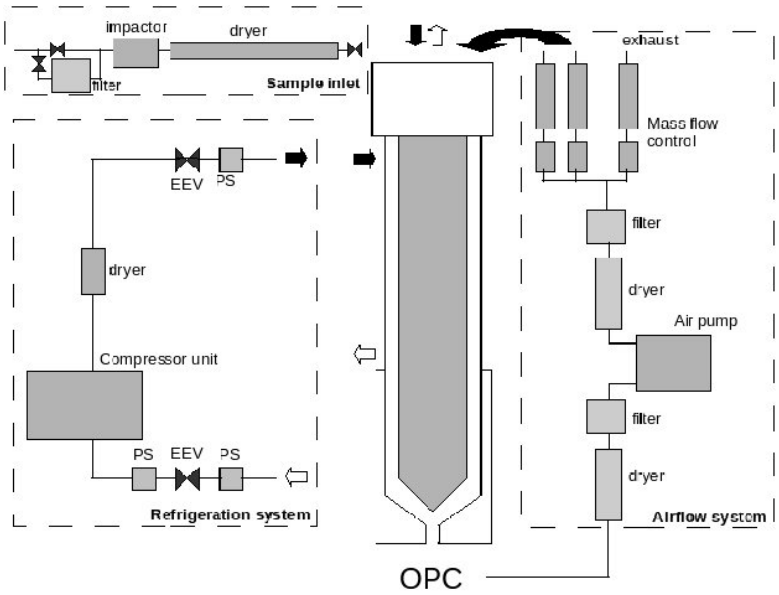

Fig. 1. Schematic of the MINC instrument separated into different systems: sample inlet, airflow system, refrigeration system and the chamber. Black lines indicate flow of air/refrigerant. Black and white arrows for the refrigeration system, match up with those indicated on the chamber, where both system inlets (inner and outer wall) are indicated. PS = pressure sensor, EEV = electronic expansion valve, see main text for description. Mass flow controls consist of an electronic flow meter and a visual flow valve. OPC = optical particle counter, see main text for details.

ACPD
10, 19277–19307, 2010

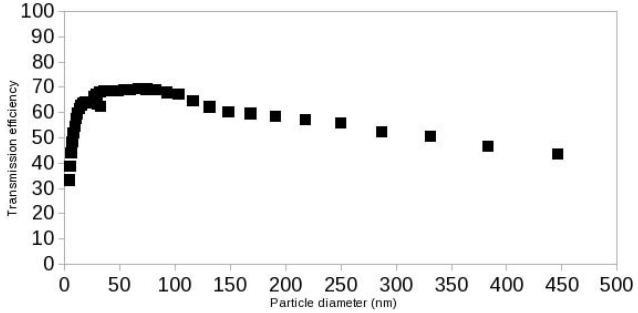

Fig. 2. Transmission curve of aerosol particles through the MINC inlet system, measured using a DMPS system. Calibration of inlet aerosol losses is based on this curve, see main text for details.

ACPD
10, 19277–19307, 2010

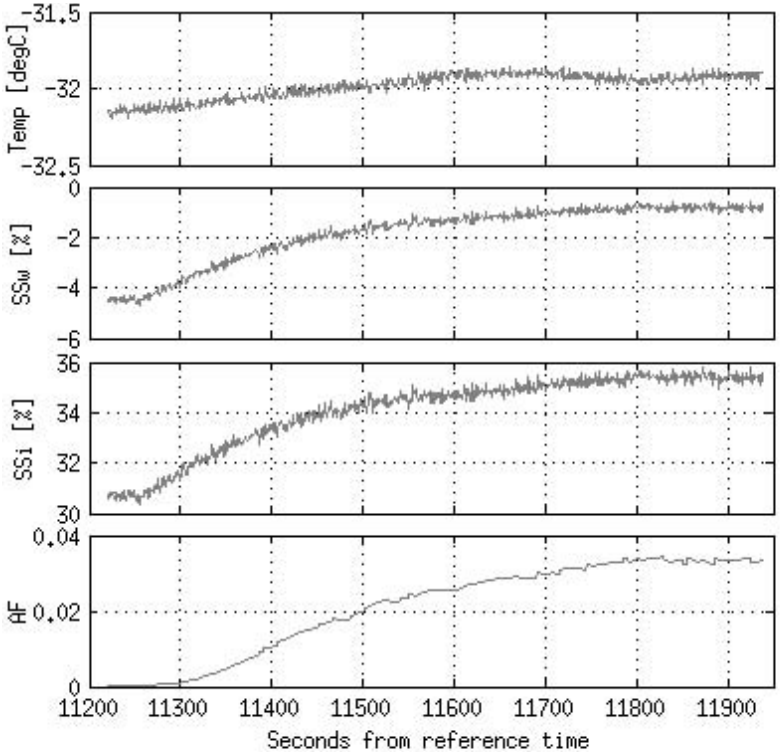

Fig. 3. Time series of calculated sample temperature (top), supersaturation with respect to ice and water (middle) and number of particles >3 µm detected (bottom) during a RH-scan. Test sample was Arizona Test Dust.

ACPD
10, 19277–19307, 2010

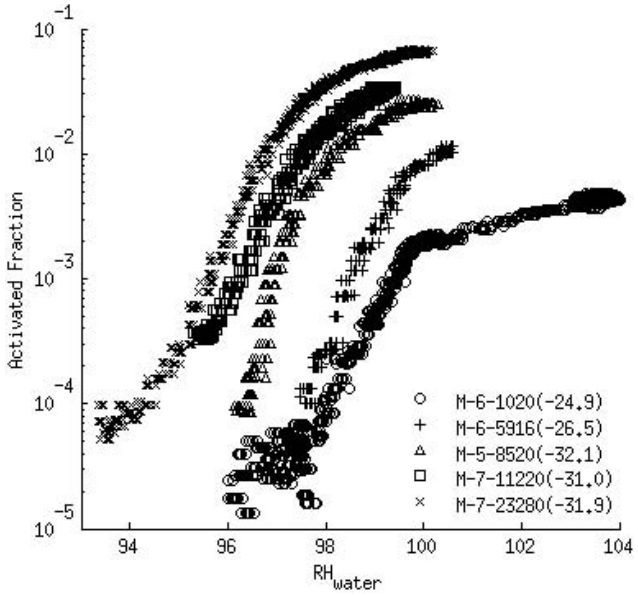

Fig. 4. Arizona test dust RH-scans performed by the MINC instrument at sample temperatures indicated by the legend.

ACPD
10, 19277–19307, 2010


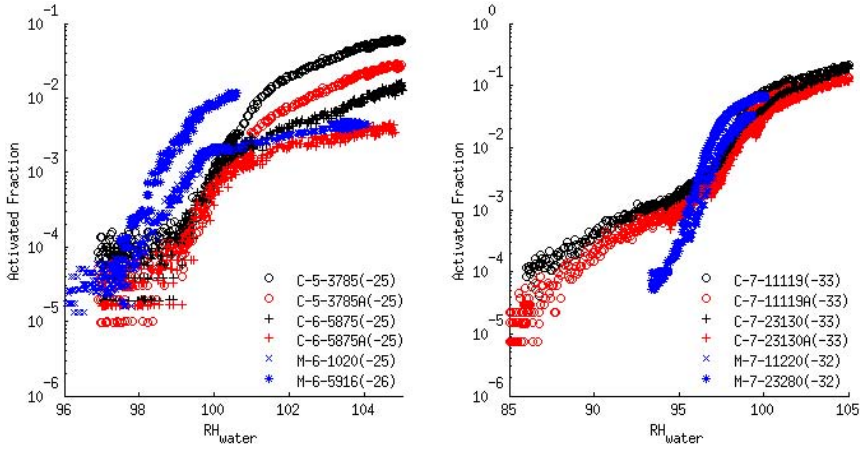

Fig. 5. Arizona test dust RH-scans. MINC results are shown in blue, CSU-CFDC results are shown in black (2 µm threshold) and red (3 µm threshold). The legends denotes the sample temperature for each RH-Scan. Results are shown for **(a)** Sample temperature ∼−26 °C, and **(b)** Sample temperature ∼−31 °C.

ACPD
10, 19277–19307, 2010

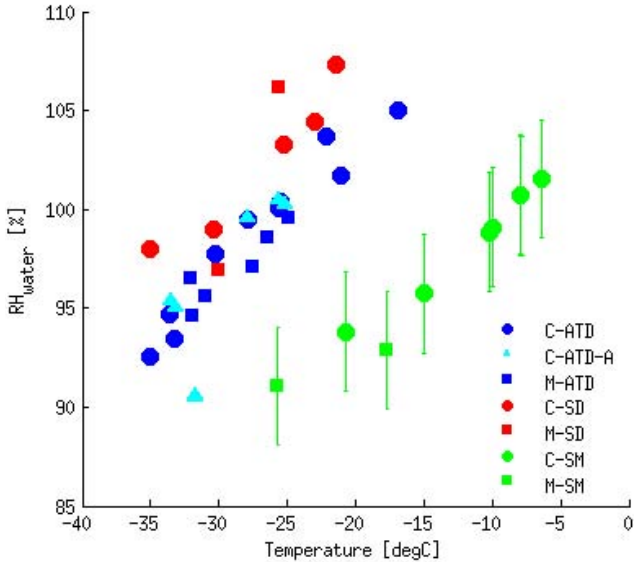

Fig. 6. Results from all MINC (circles) and CSU (squares) RH-scans for Arizona Test Dust (blue), Saharan Test Dust (red) and Snomax® (green). Points represent the conditions at which the 1 in 1000 particles were activated. CSU adjusted data points are also shown (cyan triangles). RH_{water} error bars are shown for Snomax® data (based on Richardson et al., 2010).

ACPD
10, 19277–19307, 2010

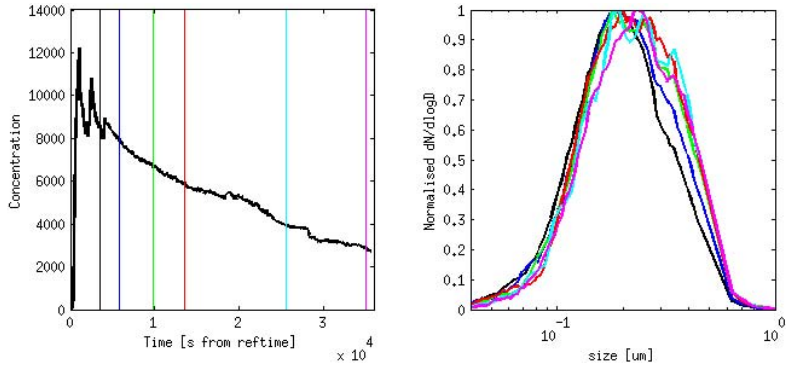

Fig. 7. Total aerosol concentration time series during 19/07/09 (left) with vertical lines representing the times at which the size distributions were taken shown (right). Size distributions are shown for times 3420, 5820, 9790, 13 500, 25 600, 35 000 seconds from the reference time.

ACPD
10, 19277–19307, 2010